NMR Characterization of Phosphonic Acid Capped SnO₂ Nanoparticles

Gregory P. Holland,*,† Ramesh Sharma,† Jacob O. Agola,‡ Samrat Amin,‡
Virgil C. Solomon,† Poonam Singh,‡ Daniel A. Buttry,‡ and Jeffery L. Yarger*,†

*Department of Chemistry and Biochemistry, Arizona State University, Tempe, Arizona 85287-1604, and
Department of Chemistry (3838), 1000 East University Avenue, University of Wyoming,
Laramie, Wyoming 82071*

Phosphonic acid capped SnO₂ nanoparticles with diameters less than 5 nm were synthesized and characterized with multinuclear solution and solid-state magic angle spinning (MAS) NMR. Two types of phosphonic acid ligands were used to derivatize the SnO₂ surface, producing (i) water soluble SnO₂ nanoparticles capped with 2-carboxyethanephosphonic acid (CEPA) and (ii) insoluble SnO₂ nanoparticles capped with phenylphosphonic acid (PPA). Multiple surface environments were observed with ³¹P solution and solid-state MAS NMR for both capping agents. The ³¹P resonances of derivatized SnO₂ nanoparticles display isotropic chemical shifts that are more shielded compared to the native phosphonic acids. This observation is indicative of a strong interaction between the phosphonic acid group and the SnO₂ surface. ¹H MAS NMR spectra display a complete absence of the acidic protons of the phosphonic acid groups, strongly supporting the formation of P−O−Sn linkages. ¹H → ³¹P cross polarization (CP) build-up behavior confirms the absence of the vast majority of phosphonic acid protons. Some of the build-up curves displayed oscillations that could be fit to extract the magnitude of the ¹H−³¹P dipolar coupling constant. The dipolar coupling can then be used to calculate the distance between phosphorus and the close proximity protons. The results presented herein indicate primarily bi- and tridentate phosphonic acid bonding configuration at the SnO₂ surface, in both CEPA and PPA capped nanoparticles.

Introduction

Confining materials to the nanometer length scale has garnered significant attention in recent years because of the large surface areas attainable and the discovery of the quantum confinement effect.[1−4] The vast majority of studies available focus on characterization of the crystalline nanoparticle core that can be readily examined with X-ray diffraction (XRD), transmission electron microscopy (TEM), and optical methods. These techniques allow for the visualization and the structural characterization of the inorganic component, and numerous studies on metal,[5,6] metal oxide,[7,8] and semiconducting[3,4] nanoparticles have appeared. The ligand environment at the nanoparticle interface is important for numerous reasons and has been studied to a much lesser extent.[9,10] Specifically, the passivating ligand is often responsible for controlling the nanoparticle growth and size. Therefore, it is related to the surface area and size dependent electronic and optical properties. In the present work, multinuclear NMR is used to characterize the ligand structural environment in phosphonic acid capped crystalline SnO₂ nanoparticles.

Nanostructured tin oxides have numerous applications including as photovoltaics,[11,12] in catalysis,[13] as transparent electrode materials[14] (in an indium doped state), in gas sensor technology,[15,16] and as anodes for lithium rechargeable batteries.[17,18] In the two latter applications, the performance

*To whom correspondence should be addressed. E-mail: jeff.yarger@asu.edu (J.L.Y.), greg.holland@asu.edu (G.P.H.).

† Arizona State University.

‡ University of Wyoming.

(1) Rossetti, R.; Nakahara, S.; Brus, L. E. *J. Chem. Phys.* **1983**, *79*, 1086−1088.

(2) Rossetti, R.; Ellison, J. L.; Gibson, J. M.; Brus, L. E. *J. Chem. Phys.* **1984**, *80*, 4464−4469.

(3) Alivisatos, A. P. *Science* **1996**, *271*, 933.

(4) Alivisatos, A. P. *J. Phys. Chem.* **1996**, *100*, 13226−13239.

(5) Schmid, G. *Chem. Rev.* **1992**, *92*, 1709−1727.

(6) Daniel, M.-C.; Astruc, D. *Chem. Rev.* **2004**, *104*, 293−346.

(7) Cushing, B. L.; Kolesnichenko, V. L.; O'Connor, C. J. *Chem. Rev.* **2004**, *104*, 3893−3946.

(8) Fernández-García, M.; Martínez-Arias, A.; Hanson, J. C.; Rodriguez, J. A. *Chem. Rev.* **2004**, *104*, 4063−4104.

(9) Tomaselli, M.; Yarger, J. L.; Bruchez, M.; Havlin, R. H.; deGraw, D.; Pines, A.; Alivisatos, A. P. *J. Chem. Phys.* **1999**, *110*, 8861−8864.

(10) Ratcliffe, C. I.; Yu, K.; Ripmeester, J. A.; Zaman, B.; Badarau, C.; Singh, S. *Phys. Chem. Chem. Phys.* **2006**, *8*, 3501−3519.

(11) Park, N.-G.; Kang, M. G.; Kim, K. M.; Ryu, K. S.; Chang, S. H.; Kim, D.-K.; Van de Lagemaat, J.; Benkstein, K. D.; Frank, A. J. *Langmuir* **2004**, *20*, 4246−4253.

(12) Hasobe, T.; Imahori, H.; Kamat, P. V.; Fukuzumi, S. *J. Am. Chem. Soc.* **2003**, *125*, 14962−14963.

(13) Wang, S.; Huang, J.; Zhao, Y.; Wang, S.; Wu, S.; Zhang, S.; Huang, W. *Mater. Lett.* **2006**, *60*, 1706−1709.

(14) Goebbert, C.; Bisht, H.; Al-Dahoudi, N.; Nonninger, R.; Aegerter, M. A.; Schmidt, H. *J. Sol-Gel Sci. Technol.* **2000**, *19*, 201−204.

(15) Williams, G.; Coles, G. S. V. *Mater. Res. Soc. Bull.* **1999**, *24*, 25−29.

(16) Martinelli, G.; Carotta, M. C.; Traversa, E.; Ghiotti, G. *Mater. Res. Soc. Bull.* **1999**, *24*, 30−36.

(17) KIm, C.; Noh, M.; Choi, M.; Cho, J.; Park, B. *Chem. Mater.* **2005**, *17*, 3297−3301.

(18) Ahn, H.-J.; Choi, H. C.; Park, K.-W.; Kim, S.-B.; Sung, Y.-E. *J. Phys. Chem. B* **2004**, *108*, 9815−9820.

of the device was greatly enhanced by decreasing the particle size to the nanometer length scale. Sol−gel chemistry is well suited for the synthesis of metal oxide nanomaterials, and a recently published SnO_2 sol−gel approach was used to synthesize the SnO_2 nanoparticles in this study.[19] The resulting SnO_2 nanoparticles were then derivatized with two types of phosphonic acid capping agents: (i) 2-carboxyethanephosphonic acid (CEPA) and (ii) phenylphosphonic acid (PPA).

TEM and atomic force microscopy (AFM) were used to determine the nanoparticle size and crystalline core, while NMR was implemented as the primary characterization tool for the phosphonic acid capping environment at the SnO_2 interface. In the solid state, ^1H magic angle spinning (MAS) and $^1H \rightarrow {}^{31}P$ cross polarization (CP)-MAS NMR provided insight into the ligand structure and extent of phosphonic acid protonation upon binding the nanoparticle surface. $^1H \rightarrow {}^{31}P$ CP build-up kinetics further elucidated the phosphonic acid binding modes at the interface. The CEPA capped SnO_2 nanoparticles are terminated with a carboxylic acid functional group making them soluble in aqueous solution. This allowed for complementary NMR characterization in the solution state.

Experimental Section

Materials. Tin isopropoxide ($Sn(O^iPr)_4PrOH$) and CEPA (Tech grade, 94%) were obtained from Alfa Aesar. Because $Sn(O^i-Pr)_4PrOH$ is hygroscopic, it was always handled and stored in an inert atmosphere. Absolute ethanol, acetylacteone (AcacH), p-toluenesulfonic acid (PTSA), potassium hydroxide (KOH), acetone (99.9%), anhydrous diethyl ether (99.9%), D_2O (99.9%), and PPA (99.9%) were obtained from Aldrich-Sigma. While the rest of the materials were used as received, absolute ethanol was dried according to the method described by Lund and Bjerrum[20] prior to use.

Synthesis of Colloidal SnO_2 Nanoparticles. Colloidal SnO_2 nanoparticles were prepared on the basis of a slight modification of the method introduced by de Monredon et al.[19] Briefly, 1 g of $Sn(O^iPr)_4PrOH$ was dissolved in 10 g of absolute ethanol under argon gas. Four grams of AcacH were added through a septum under magnetic stirring to achieve a complexant ratio ($A = AcacH/Sn$) of 4. This mixture was stirred for 2 h before hydrolysis was performed under magnetic stirring by slowly adding 1 mL of 2 M PTSA prepared in Millipore water such that the hydrolysis ratio ($H = H_2O/Sn$) was 10 and the acidity ratio ($R = PTSA/Sn$) was 0.4. After stirring the mixture for 2 h at room temperature, the solution was transferred to a glass container, tightly sealed, and aged for 24 h in an oven at 60 °C. Solid nanoparticles were obtained from the colloid by heating it under vacuum in an oven at the same temperature. A liquid nitrogen trap was used to avoid contamination. This preparation was repeated 10 times, producing nanoparticles with an average diameter of 3.5 ± 2.0 nm.

Capping of SnO_2 Nanoparticles with Phosphonic Acids. Surface modification of SnO_2 nanoparticles was accomplished using CEPA and PPA. Capping with CEPA was done taking into consideration the different pK_a values of the acidic protons.[21,22] Ten grams of the SnO_2 colloidal solution was transferred to a round-

bottom flask followed by addition of a 25 mL solution of 0.08 M CEPA and 3 molar equiv of KOH (60 mL of 0.1 M KOH). The pH of the solution was measured and found to be ∼5.5. The mixture was then heated at 70 °C for 3 days. The solution remained completely transparent during the heating process.

The solid CEPA capped SnO_2 nanoparticles were recovered using a centrifuge (15 000 rpm for 45 min). The nanoparticles were then washed by vigorously sonicating in 40 mL of solvent (ethanol, acetone, and anhydrous diethyl ether) for 5 min followed by intermittent centrifugation (15 000 rpm for 20 min). This is similar to the procedure used to wash CEPA capped TiO_2 and ZrO_2 nanoparticles.[23,24] In each washing step, the supernatant was removed and the next solvent added. The complete washing process was performed in the following order: five times with ethanol, once with acetone, and once with anhydrous diethyl ether. The washed, surface modified SnO_2 nanoparticles were dried by purging with argon gas followed by treatment in a vacuum oven at 150 °C for 15 h.

Surface modification of SnO_2 nanoparticles with PPA was conducted in a similar fashion with the following modifications. The SnO_2 colloidal solution was adjusted to a pH of ∼5 using 50 mL of 0.1 M KOH before adding 0.234 g of PPA. The mixture was heated at 70 °C similar to the CEPA route. The solution appeared cloudy during the heating period. The washing of recovered PPA capped SnO_2 nanoparticles was carried out using the same steps as the CEPA capped case with the following alteration in the order of washing: four times with ethanol, once with the $EtOH/H_2O$ (3:1) mixture, once with acetone, and once with anhydrous diethyl ether. Unlike the CEPA capped SnO_2 nanoparticles, the PPA capped ones did not dissolve in any of the solvents during the washing steps. The PPA capped nanoparticles were dried the same as the CEPA capped nanoparticles. After a series of attempts, none of the available solvents could dissolve PPA capped SnO_2 nanoparticles.

Dialysis of CEPA Capped SnO_2 Nanoparticles. Dialysis was performed in Millipore water using dialysis membrane tubing (Spectra/Por molecular porous membrane tubing) with a pore size of 2−3 nm and molecular weight cut off (MWCO) of 12 000−14 000 Da to remove any additional impurities that remained following the washing steps. Water (900 mL) for dialysis was changed several times throughout the process. This was useful for the removal of excess phosphonic acid and other unbound impurities and greatly improved the quality of the microscopy images.

Synthesis of Deuterated Phosphonic Acids. Deuterated CEPA (d2-CEPA) and PPA (d2-PPA) samples were prepared by slowly recrystallizing the as-received phosphonic acid three times from a solution of 99.9% D_2O resulting in deuteration of the exchangeable acidic protons.

TGA. Thermal gravimetric analysis (TGA) was performed with a Setaram TG 92 scanning from 20 °C to 600 °C at a rate of 10 °C/min under a He atmosphere. Total weight loss was monitored as a function of temperature.

TEM. High-resolution TEM and energy dispersive X-ray (EDX) spectroscopy were employed for microstructural characterization and microanalysis of dialyzed CEPA capped SnO_2 nanoparticles. The TEM samples were dispersed in water by sonication and drop-pipetted onto a lacey carbon film supported by a copper grid (Ted Pella, Inc.). The sample was allowed to dry in air before imaging in the electron microscope. The high-resolution images were

(19) de Monredon, S.; Cellot, A.; Ribot, F.; Sanchez, C.; Armelao, L.; Gueneau, L.; Delattre, L. *J. Mater. Chem.* **2002**, *12*, 2396−2400.
(20) Lund, H.; Bjerrum, J. *Ber. Dtsch. Chem. Ges.* **1931**, *64B*, 210.
(21) Ohta, K. *Bull. Chem. Soc. Jpn.* **1992**, *65*, 2543−2545.

(22) Heubel, P. C.; Popov, A. I. *J. Solution Chem.* **1979**, *8*, 615−625.
(23) Pawsey, S.; McCormick, M.; De Paul, S.; Graf, R.; Lee, Y. S.; Reven, L.; Spiess, H. W. *J. Am. Chem. Soc.* **2003**, *125*, 4174−4184.
(24) Pawsey, S.; Yach, K.; Reven, L. *Langmuir* **2002**, *18*, 5205−5212.

recorded with a JEOL JEM-2010F field emission gun electron microscope operated at 200 kV with a point resolution of 1.9 Å. The instrument is equipped with a slow-scan CCD camera (Gatan model 694), an EDX detector (EDAX), and Gatan-Digital Micrograph and EDAX-Genesis acquisition systems.

AFM. Dialyzed CEPA capped SnO₂ nanoparticles (10^{-9} M solution in Millipore water) were deposited on a highly oriented pyrolytic graphite (HOPG) substrate using a drop coating technique and subsequently dried for 15 min. Noncontact AFM was then carried out using phosphorus doped silicon cantilevers (Veeco, model RTESPA-M) with a force constant of 20−80 N/m with a Veeco CP II scanning probe microscope.

NMR. ^{1}H and ^{31}P solution NMR were collected on a Varian Inova 500 spectrometer equipped with a 5 mm Varian indirect-detection PFG liquids probe operating at 500.0 and 202.5 MHz, respectively. ^{1}H solution spectra were collected with a 5 s recycle delay. ^{31}P spectra were obtained with a recycle delay of 60 s and ^{1}H decoupling during acquisition. Spin−spin relaxation (T_2) measurements were performed with a spin−echo pulse sequence.[25] The ^{1}H and ^{31}P solution NMR spectra were referenced to trimethyl silane (TMS) and 85% phosphoric acid, respectively.

Solid state ^{1}H MAS and ^{1}H → ^{31}P CP-MAS NMR spectra were obtained on a Varian Inova 400 spectrometer equipped with a 4 mm Jacobsen double resonance CP-MAS probe at 10 kHz MAS for ^{31}P detected experiments and 15 kHz MAS for ^{1}H experiments. In the pure phosphonic acids, the ^{31}P CP-MAS spectra were collected with four scans and a recycle delay that was typically 90 s. The ^{1}H T_1 relaxation time in these strongly hydrogen bonded solids is in excess of 3 min as approximated by inversion recovery methods. The ^{1}H $\pi/2$ pulse lengths were 4.0 μs in ^{1}H MAS experiments and 4.5 μs for ^{31}P CP-MAS experiments. In the CP experiments, the ^{1}H RF field strength was 56 kHz and ^{31}P was matched to the first spinning sideband ($\pm$1) in the Hartmann−Hahn matching profile, corresponding to a field strength of 46 kHz for ^{31}P at 10 kHz MAS. High power ^{1}H decoupling was applied during acquisition (50 kHz RF field strength). The ^{1}H and ^{13}P NMR spectra were referenced in the solid state to TMS and 85% phosphoric acid indirectly by setting the ^{1}H resonance of adamantane (δ = 1.63 ppm) and ^{31}P resonance of NH₄PO₄H₂ (δ = 0.8 ppm), respectively. The remaining experimental parameters such as the CP contact times for individual experiments are indicated in the figure captions. ^{1}H → ^{31}P CP build-up curves were obtained as a function of contact time, and the curves were fit with two models: (1) the classic I−S model and (2) the I−I*−S model. The latter model accounts for dipolar oscillations that result from coherent polarization transfer and the impact of ^{1}H spin diffusion.[26−31] The equations for these two models are given below:

$$I(t) = I_0\left(1 - \frac{T_{IS}}{T_{1\rho}^I}\right)^{-1}\left[\exp\left(-\frac{t}{T_{1\rho}^I}\right) - \exp\left(-\frac{t}{T_{IS}}\right)\right] \quad (1)$$

$$I(t) = I_0\exp\left(-\frac{t}{T_{1\rho}^I}\right)\left[1 - \frac{1}{2}\exp\left(-\frac{t}{T_{df}}\right) - \frac{1}{2}\exp\left(-\frac{3t}{2T_{df}}\right)\cos\left(\frac{bt}{2}\right)\right] \quad (2)$$

where I, t, T_{IS}, $T_{1\rho}^I$, T_{df}, and b are the CP intensity, contact time, CP rate constant, ^{1}H spin−lattice relaxation time in the rotating frame, ^{1}H spin-diffusion rate constant, and the dipolar coupling between the ^{1}H−^{31}P spin pair, respectively.[32] Equation 1 assumes that the ^{1}H population greatly exceeds the ^{31}P population and $T_{IS}/T_{1\rho}^S \approx 0$, where $T_{1\rho}^S$ is the ^{31}P spin−lattice relaxation time in the rotating frame. Equation 2 assumes very slowly relaxing ^{31}P spins ($T_{1\rho}^S = \infty$) and isotropic ^{1}H spin-diffusion where the rate of isotropic proton spin diffusion, $3R$ ($R = 1/T_{df}$), greatly exceeds $1/T_{1\rho}^I$. The dipolar coupling constant, $D = b/(2\pi)$, extracted from the fit of the build-up curves with eq 2, is scaled by a factor of $\sqrt{2}$ for a $\pm$1 spinning sideband CP matching condition.[33−36] This scaling factor was accounted for in the reported values of D.

Results and Discussion

TEM and AFM. Images of CEPA capped SnO₂ nano-particles obtained with TEM and AFM are presented in Figure 1 along with the molecular structure of the CEPA and PPA capping ligand. The TEM image (Figure 1a) indicates a high degree of crystallinity for the spherical nanoparticle core with typical particle diameters < 5 nm. This is in agreement with XRD results where a broadened diffraction pattern characteristic of SnO₂ having a cassiterite structure was used to calculate an average particle size of ∼2.0 nm (data not shown). EDX spectra, obtained in conjunction with TEM, contained signals from Sn, O, C, and P consistent with the core and ligand structure of the CEPA capped SnO₂ nanoparticles (see Supporting Information, Figure S1). Typical AFM images (Figure 1b) also indicate isolated nanoparticles with sizes ranging from 1.2 to 2.5 nm, as measured from the nanoparticle heights.

Solution NMR. The CEPA capped SnO₂ nanoparticles are soluble in aqueous solutions permitting characterization via solution NMR. This is in stark contrast to the PPA capped nanoparticles that were insoluble in aqueous solutions and standard organic solvents. This presumably results from the difference in terminal functional group where the carboxylic acid makes the CEPA capped SnO₂ nanoparticles soluble in polar solvents, while the phenyl ring of the PPA capped samples renders them essentially insoluble. The unexpected insolubility of PPA capped nanoparticles in toluene suggests strong interactions between nanoparticles that drive their aggregation.

The ^{1}H solution NMR spectra of CEPA and CEPA capped SnO₂ nanoparticles dissolved in D₂O are shown in Figure 2. The ^{1}H resonances of the acidic protons (carboxylic or phosphonic), if present, will not be observed because they will readily exchange with the D₂O solvent. The CH₂ protons are observed in the pure CEPA sample (Figure 2a) at 1.7

(25) Hahn, E. L. *Phys. Rev.* **1950**, *80*, 580−594.
(26) Müller, L.; Kumar, A.; Baumann, T.; Ernst, R. R. *Phys. Rev. Lett.* **1974**, *32*, 1402−1406.
(27) Hester, R. K.; Ackerman, J. L.; Cross, V. R.; Waugh, J. S. *Phys. Rev. Lett.* **1975**, *34*, 993−995.
(28) Naito, A.; McDowell, C. A. *J. Chem. Phys.* **1986**, *84*, 4181−4186.
(29) Levitt, M. H.; Suter, D.; Ernst, R. R. *J. Chem. Phys.* **1986**, *84*, 4243−4255.
(30) Takegoshi, K.; McDowell, C. A. *J. Chem. Phys.* **1987**, *86*, 6077−6084.
(31) Hagaman, E. W.; Ho, P. C.; Brown, L. L.; Schell, F. M.; Woody, M. C. *J. Am. Chem. Soc.* **1990**, *112*, 7445−7450.
(32) Kolodziejski, W.; Klinowski, J. *Chem. Rev.* **2002**, *102*, 613−628.
(33) Bertani, B.; Raya, J.; Reinheimer, P.; Gougeon, R.; Delmotte, L.; Hirschinger, J. **1999**, *13*, 219−229.
(34) Azaïs, T.; Bonhomme, C.; Bonhomme-Coury, L.; Vaissermann, J.; Millot, Y.; Man, P. P.; Bertani, B.; Hirschinger, J.; Livage, J. *J. Chem. Soc., Dalton Trans.* **2002**, *4*, 609−618.
(35) Azaïs, T.; Bonhomme-Coury, L.; Vaissermann, J.; Bertani, B.; Hirschinger, J.; Maquet, J.; Bonhomme, C. *Inorg. Chem.* **2002**, *41*, 981−988.
(36) Hologne, M.; Bertani, B.; Azaïs, T.; Bonhomme, C.; Hirschinger, J. *Solid State Nucl. Magn. Reson.* **2005**, *28*, 50−56.
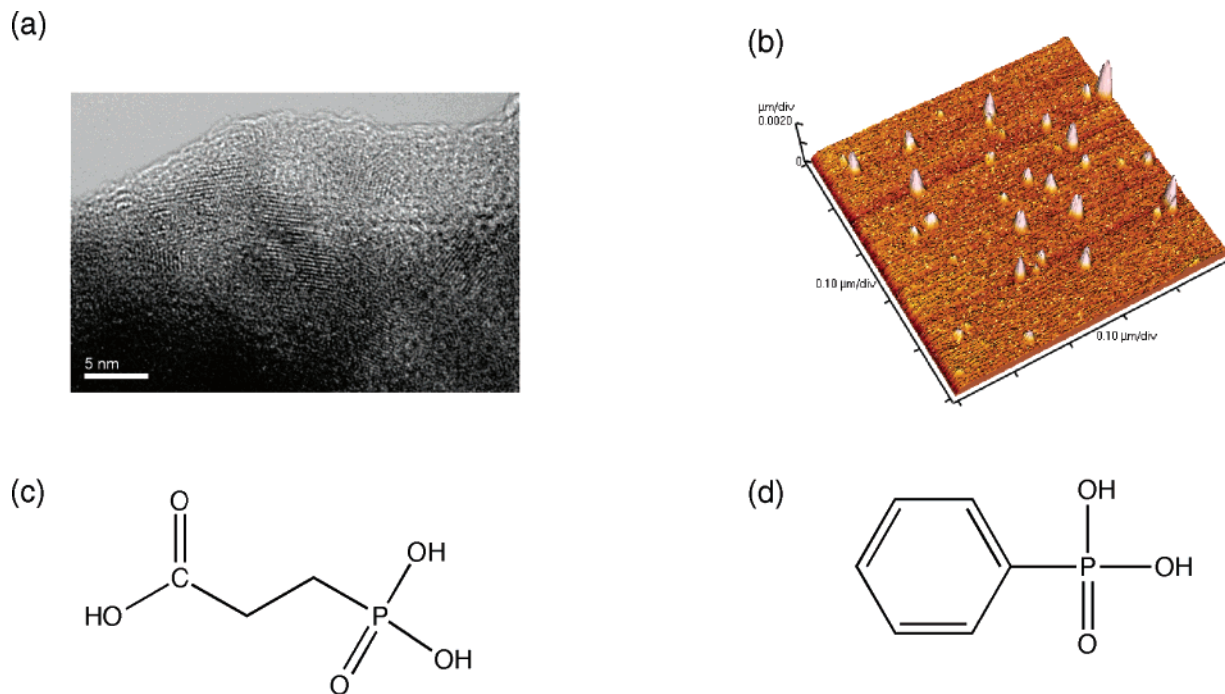
(a)

(b)

(c)

(d)

Figure 1. (a) TEM and (b) AFM images of CEPA capped SnO_2 nanoparticles. The molecular structure of (c) CEPA and (d) PPA ligand capping agents.
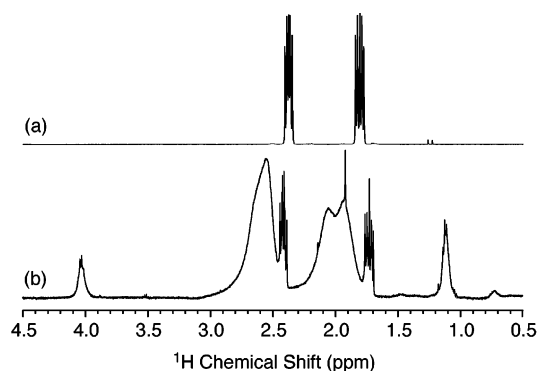

Figure 2. ^1H solution NMR spectrum of (a) CEPA and (b) CEPA capped SnO_2 nanoparticles dissolved in D_2O.

and 2.4 ppm corresponding to the CH_2 groups adjacent to the phosphonic and carboxylic acids, respectively. These two resonances are extensively split by a combination of $^1H-$ ^1H and $^1H-^{31}P$ J couplings. For the CEPA capped SnO_2 nanoparticles (Figure 2b), two pairs of CH_2 resonances are observed: a narrow set similar to that of the pure CEPA sample (Figure 2a) and a broad set that is shifted downfield. The broad resonances can be assigned to the CEPA ligands bound to the SnO_2 nanoparticles, while the narrower set is assigned to free ligand. The relative ratio of free to bound CEPA ligands is 11% on the basis of integration of the sharp and broad CH_2 resonances, respectively. Broadened ^1H resonances are also observed that can be ascribed to residual, bound acetylacetonate ligands at 1.1 and 4.0 ppm corresponding to the CH_3 and CH groups, respectively. This line broadening of ligand capping agents has been observed in ^1H and ^{13}C solution state NMR spectra of Au nanoparticles capped with alkylthiol and phosphine ligands.[37-40] There are

two mechanisms typically proposed for this observed line broadening in the solution NMR spectra of capped nanoparticles: (1) residual dipolar coupling reintroduced because the nanoparticle rotates slower than the time required for isotropic averaging of the dipolar coupling[37] and (2) chemical shift heterogeneity resulting from a distribution of chemical environments at the nanoparticle interface and/or a distribution in particle size.[40,41] Hole-burning[42] experiments performed on a ^{13}C CP-MAS NMR spectrum of alkylthiol capped Au nanoparticles showed that the C-2 resonance (second closest to the Au interface) was inhomogeneously broadened supporting the latter mechanism in the solid sample.[41] It was confirmed that the line broadening in the ^1H solution state spectra of the SnO_2 nanoparticles is primarily inhomogeneous in nature by hole-burning experiments (see Supporting Information, Figure S2). This strongly supports chemical shift heterogeneity as the main cause for the broadening. The measured T_2 relaxation time of these two broad resonances is 9−10 ms predicting an 30−35 Hz line width assuming a Lorentzian line shape. The observed line width of the resonance at 2.4 ppm is ∼800 Hz, confirming chemical shift heterogeneity as the primary contribution to the line width. It is interesting to point out that the hole burnt in this resonance is 30 Hz wide consistent with the T_2 measurement. The downfield chemical shift and broadening of these resonances indicate that these CEPA molecules remain strongly bound to the

(37) Terrill, R. H.; Postlethwaite, T. A.; Chen, C.-h.; Poon, C.-D.; Terzis, A.; Chen, A.; Hutchinson, J. E.; Clark, M. R.; Wignall, G.; Londono, J. D.; Superfine, R.; Falvo, M.; Johnson, C. S.; Samulski, E. T.; Murray, R. W. *J. Am. Chem. Soc.* **1995**, *117*, 12537−12548.

(38) Badia, A.; Gao, W.; Singh, S.; Demers, L.; Cuccia, L.; Reven, L. *Langmuir* **1996**, *12*, 1262−1269.
(39) Weare, W. W.; Reed, S. M.; Warner, M. G.; Hutchinson, J. E. *J. Am. Chem. Soc.* **2000**, *122*, 12890−12891.
(40) Zelakiewicz, B. S.; de Dios, A. C.; Tong, Y. Y. *J. Am. Chem. Soc.* **2002**, *125*, 18−19.
(41) Badia, A.; Demers, L.; Dickinson, L.; Morin, F. G.; Lennox, R. B.; Reven, L. *J. Am. Chem. Soc.* **1997**, *119*, 11104−11105.
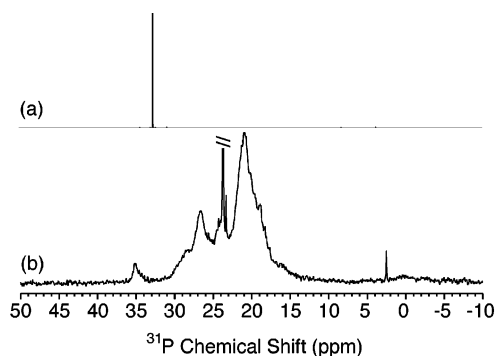(42) Bloembergen, N.; Purcell, E. M.; Pound, R. V. *Phys. Rev.* **1948**, *73*, 679−712.

Figure 3. ^{31}P solution NMR spectrum of (a) CEPA and (b) CEPA capped SnO₂ nanoparticles dissolved in D₂O.

SnO₂ surface when the nanoparticles are dissolved in solution and signify successful capping.

The phosphonic acid group was probed in solution with ^{31}P NMR, and the spectra of pure CEPA and CEPA capped SnO₂ nanoparticles dissolved in D₂O are depicted in Figure 3. The native CEPA sample has a single sharp isotropic resonance positioned at 32.7 ppm whereas the CEPA capped nanoparticles display a complex, broadened spectrum with multiple resonances that are primarily shifted upfield. These resonances are broadened similar to the ^{1}H solution NMR resonances consistent with ligand attachment to the SnO₂ surface. The observation of an upfield ^{31}P chemical shift when phosphonic acids are bound to metal oxides,[23,24,43−46] silica,[47,48] and functionalized silica[49] surfaces has been previously reported in a number of studies where ^{31}P MAS or CP-MAS was used to investigate the materials in the solid state. This is the first study that has demonstrated the presence of intact phosphonic acid linkages to an oxide surface in solution to the best of our knowledge. It should also be noted that the ^{31}P resonance of the free ligand is positioned at 27.7 ppm in the solution spectrum of the CEPA capped SnO₂ nanoparticles and the relative ratio of free to bound ligand is 13% in close agreement with the ^{1}H solution NMR results discussed above.

The ^{31}P chemical shift observed for the free ligand is ∼5 ppm upfield from the position of the pure CEPA resonance. This is a result of deprotonation of the free ligand due to the pH of the nanoparticle solution. The pH values of solutions of CEPA and CEPA capped nanoparticles were 1 ± 1 and 5 ± 1, respectively. The pH dependence of the ^{31}P chemical shift of phosphorus oxyacids has been well documented in the literature where more negative ^{31}P chemical shifts were observed with increasing pH.[50] Addition of CEPA to the nanoparticle solution caused the free ligand resonance to shift downfield toward the pure CEPA reso-
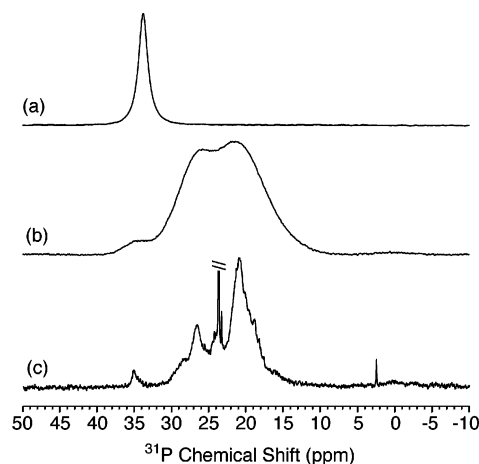
(43) Gao, W.; Dickinson, L.; Grozinger, C.; Morin, F. G.; Reven, L. *Langmuir* **1996**, *12*, 6429−6435.
(44) Neff, G. A.; Page, C. J.; Meintjes, E.; Tsuda, T.; Pilgrim, W.-C.; Roberts, N.; Warren, W. W. *Langmuir* **1996**, *12*, 238−242.
(45) Guerrero, G.; Mutin, P. H.; Vioux, A. *Chem. Mater.* **2000**, *12*, 1268−1272.
(46) Guerrero, G.; Mutin, P. H.; Vioux, A. *Chem. Mater.* **2001**, *13*, 4367−4373.
(47) Lukeš, I.; Borbaruah, M.; Quin, L. D. *J. Am. Chem. Soc.* **1994**, *116*, 1737−1741.
(48) Blümel, J. *Inorg. Chem.* **1994**, *33*, 5050−5056.
(49) Sasaki, D. Y.; Alam, T. M. *Chem. Mater.* **2000**, *12*, 1400−1407.
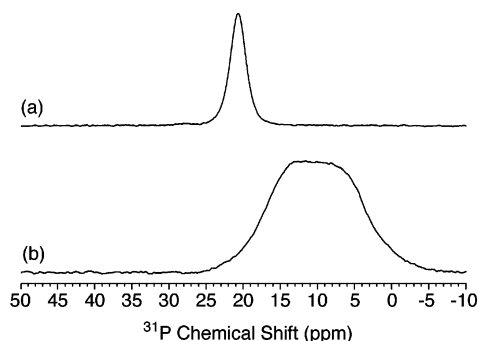(50) Moedritzer, K. *Inorg. Chem.* **1967**, *6*, 936−939.

Figure 4. ^{31}P CP-MAS NMR collected at 10 kHz with a 1 ms contact time for (a) CEPA and (b) CEPA capped SnO₂ nanoparticles. The (c) ^{31}P solution NMR spectrum is shown for comparison purposes.

Table 1. ^{31}P NMR Chemical Shifts of Pure Phosphonic Acids and Phosphonic Acid Capped SnO₂ Nanoparticles

sample	$\delta_{^{31}P}$ (ppm)	$\Delta\delta_{^{31}P}{}^{a}$ (ppm)
CEPA(aq)	32.7	
CEPA(s)	34.1	
CEPA/SnO₂(aq)	35.0, 26.6, 20.9	+2.3, −6.1, −11.8
CEPA/SnO₂(s)	35.0, 27.4, 21.0	+0.9, −6.7, −13.1
PPA(s)	21.3	
PPA/SnO₂(s)	13.9, 6.7	−7.4, −14.6

^{a} With respect to the pure phosphonic acid.

nance. Further, when an aqueous CEPA solution was prepared with a concentration matching that of the free ligand (based on the combination of TGA results [see Figure S3, Supporting Informatoin] and the ratio of free to bound ligand from integration of the ^{31}P resonances) a similar ^{31}P chemical shift and pH were observed compared to those of the nanoparticle solution.

Solid State ^{31}P CP-MAS NMR. The ^{1}H → ^{31}P CP-MAS NMR spectra of CEPA (a) and CEPA capped SnO₂ are shown in Figure 4. The ^{31}P isotropic chemical shift of the pure CEPA sample is 34.1 ppm, while the capped SnO₂ nanoparticles display three primary resonances positioned at 35.0, 27.4, and 21.0 ppm. The ^{31}P solution NMR spectrum is also presented (Figure 4c) for comparison purposes. The solution and solid state ^{31}P NMR spectra of CEPA capped SnO₂ display comparable resonances that have similar chemical shifts (see Table 1). This provides convincing evidence that the ligand linkages to the SnO₂ surface are very similar in the solid state and when they are dissolved in aqueous solutions. Again, the resonances that are shifted upfield and broadened represent phosphonic acid groups that interact strongly with the SnO₂ nanoparticle surface. The broadening likely results from chemical shift heterogeneity due to a distribution in sites at the nanoparticle interface.

In previous ^{31}P CP-MAS NMR studies on phosphonic acids reacted with silica gel surfaces, analogous ^{31}P chemical shifts of −5 ± 1 and −15 ± 1 ppm were observed compared to the chemical shift of the pure phosphonic acids.[47] These two shifts were assigned to mono- and bidentate phosphonic acid groups covalently bonded to the silica surface, respectively. Similar chemical shift variations are observed for CEPA at SnO₂ nanoparticle surfaces where the two primary

2524 *Chem. Mater., Vol. 19, No. 10, 2007*

Holland et al.

Figure 5. ^{31}P CP-MAS NMR collected at 10 kHz MAS with a 1 ms contact time for (a) PPA and (b) PPA capped SnO$_2$ nanoparticles.

resonances are shifted upfield −6.7 and −13.1 ppm from the chemical shift of pure CEPA (see Figure 4). The degree of protonation of the different sites was probed with ^{1}H MAS and ^{1}H−^{31}P CP build-up curves discussed below.

A minor component is observed at 35.0 ppm in both the ^{31}P solution and the solid-state CP-MAS NMR spectra of CEPA capped SnO$_2$ nanoparticles (see Figure 4). This ^{31}P isotropic chemical shift is near that observed for the native CEPA sample. The larger breadth of this resonance in the ^{31}P solution state spectra of the nanoparticles compared with the solution spectrum of pure CEPA (see Figure 3) indicates that this resonance is associated with the nanoparticle and is not residual CEPA. If it corresponded to residual CEPA a much sharper resonance would be expected. However, this resonance does not shift upfield in comparison to the other nanoparticle bound CEPA resonances (see Table 1). This indicates a much weaker interaction with the nanoparticle interface. A small amount of carboxylic surface interactions has been reported in previous studies on carboxyalkylphosphonic acids on ZrO$_2$ nanopowders providing one possible explanation for the appearance of a ^{31}P resonance with a chemical shift similar to pure CEPA.[24] However, CP build-up kinetics discussed below indicate that this is not the case. Therefore, this broad resonance observed at 35 ppm is assigned to CEPA molecules that interact with SnO$_2$ nanoparticles weakly via the phosphonic acid group. A minor broad component is also observed near 0 ppm that can be assigned to a small amount of residual phosphates created during the capping step or the possibility of forming a small amount of metal phosphonate.[51,52] However, the latter typically results in a sharp resonance in contrast to the broadened resonance observed in this study.

The PPA capped SnO$_2$ nanoparticles gave similar ^{31}P CP-MAS NMR results compared to the CEPA capped samples (Figure 5). A broad ^{31}P NMR resonance comprised of two components that are shifted upfield is observed. The two components display chemical shifts of −7.4 and −14.6 ppm compared to PPA. This observed change in chemical shift, $\Delta\delta$, for the PPA capped SnO$_2$ nanoparticles is larger than that for the CEPA capped samples (see Table 1). Larger upfield ^{31}P chemical shifts were proposed to indicate a stronger interaction with the metal oxide surface in the case

of phosphonic acids adsorbed on TiO$_2$ and ZrO$_2$ surfaces.[43] Thus, larger shifts observed here could provide evidence for a stronger interaction for PPA than for CEPA on SnO$_2$ nanoparticles. This is supported by TGA data (see Supporting Information, Figure S3) where the completion of PPA removal occurred at higher temperatures compared to CEPA loss from the capped SnO$_2$ nanoparticles. A slightly higher surface coverage by mass was also observed for PPA capped samples (25.6% compared to 22.5% for CEPA).

Solid State ^{1}H MAS NMR. To elucidate the amount of remaining protons at the phosphonic acid group following the capping process, ^{1}H MAS NMR was collected. The ^{1}H NMR spectra obtained with MAS at 15 kHz on CEPA, PPA, CEPA capped SnO$_2$ nanoparticles, and PPA capped SnO$_2$ nanoparticles are shown in Figure 6. At these intermediate MAS speeds, the ^{1}H−^{1}H dipolar coupling is not completely averaged. However, the resolution is sufficient to separate the acidic proton resonance (∼12 ppm) from the CH$_2$ resonance (∼3 ppm) in CEPA and the phenyl ring resonance (∼7 ppm) in PPA. In both samples, there is a significant decrease in the acidic proton resonance located between 10 and 15 ppm in the capped SnO$_2$ nanoparticles. In fact, the PPA capped SnO$_2$ displays no evidence of an acidic proton resonance indicating complete removal of these protons. In the CEPA capped sample, a broad resonance corresponding to acidic protons still remains, but these may correspond to the terminal carboxylic acid group. The ^{1}H spectrum of CEPA capped sample also exhibits a considerable change downfield of the aliphatic resonance near ∼6 ppm. This is a typical chemical shift for adsorbed water[53] that likely interacts at the terminal carboxylic acid group.

The salient feature in the ^{1}H MAS spectrum of phosphonic acid capped SnO$_2$ nanoparticles is the significant decrease of the acidic proton resonance. This can be interpreted as a removal of the OH protons. There are other possibilities for the lack of observing ^{1}H resonances that represent the remaining phosphonic acid protons in the SnO$_2$ nanoparticles: (1) the remaining phosphonic acid protons are broadened into the baseline due to chemical shift heterogeneity and/or (2) these resonances are chemically shifted and convoluted under the main CH$_2$ resonance in the case of the CEPA capped sample or under the phenyl ring resonance in PPA. The chemical shift of acidic protons in the solid state is dependent on hydrogen bond strength and can appear between 5 and 20 ppm.[54] To resolve the two latter arguments, ^{31}P CP-MAS build-up curves were obtained as a function of contact time to measure the degree of phosphonic acid protonation.

^{1}H → ^{31}P CP-MAS Build-up Kinetics. CP build-up curves collected for the pure phosphonic acids and phosphonic acid capped SnO$_2$ nanoparticles are displayed in Figure 7. Data are also shown for pure phosphonic acids where the acidic protons were exchanged for deuterium. This provides a model compound where the acidic protons are completely absent. It is clear that both the PPA and the CEPA capped SnO$_2$ nanoparticle samples display similar CP initial

(51) Burwell, D. A.; Valentine, K. G.; Thompson, M. E. *J. Magn. Reson.* **1992**, *97*, 498−510.
(52) (52) Corriu, R. J. P.; Leclercq, D.; Mutin, P. H.; Sarlin, L.; Vioux, A. *J. Mater. Chem.* **1998**, *8*, 1827−1833.

(53) Cho, G.; Wu, Y.; Ackerman, J. L. *Science* **2003**, *300*, 1123−1127.
(54) Harris, R. K.; Jackson, P.; Merwin, L. H.; Say, B. J. *J. Chem. Soc., Faraday Trans. 1* **1988**, *84*, 3649−3672.
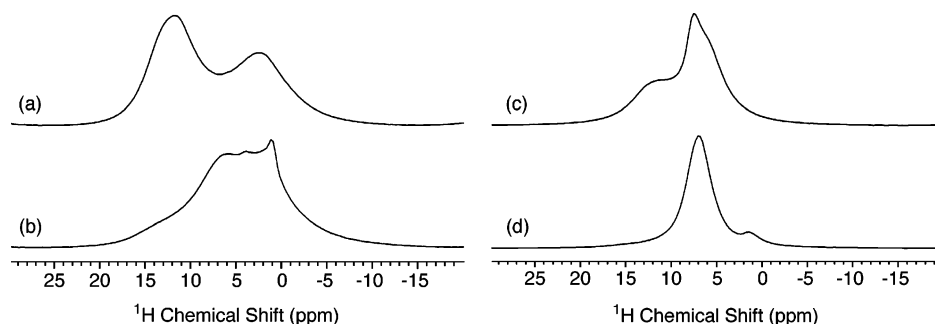
Figure 6. ¹H MAS NMR collected at 15 kHz MAS for (a) CEPA, (b) CEPA capped SnO₂ nanoparticles, (c) PPA, and (d) PPA capped SnO₂ nanoparticles.
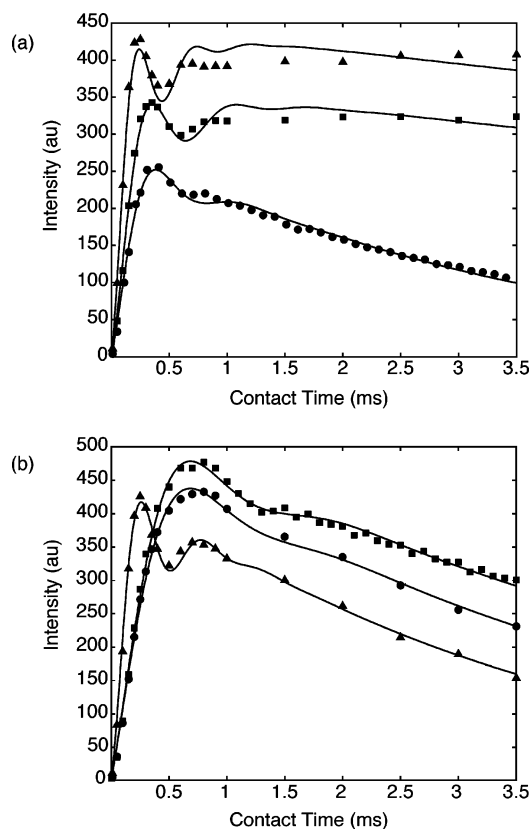

Figure 7. $^1H \rightarrow {}^{31}P$ CP build-up curves collected at 10 kHz MAS on the −1 spinning sideband in the Hartmann−Hahn matching profile. (a) CEPA (▲), d2-CEPA (■), and CEPA capped SnO₂ nanoparticles (●); (b) PPA (▲), d2-PPA (■), and PPA capped SnO₂ nanoparticles (●). Solid lines are fits with the I−I*−S model (eq 2); see Table 2 for extracted parameters.

Table 2. $^1H \rightarrow {}^{31}P$ CP Parameters Extracted from CP Build-up Curves

sample	$T_{IS}{}^a$ (μs)	D^b (kHz)	r^c (Å)	$T_{1\rho}^I$ (ms)	$T_{df}{}^b$ (μs)
PPA	230	4.94	2.15	3.1	460
d2-PPA	800	1.78	3.03	3.9	690
PPA/SnO₂	850	1.85	2.99	4.9	750
CEPA	240	5.81	2.04		370
d2-CEPA	440	3.93	2.33		500
CEPA/SnO₂	410	3.39	2.44	3.1	480

^{a} Extracted from a fit with the classic I−S model (eq 1). ^{b} Extracted from a fit with the I−I*−S model (eq 2). ^{c} Calculated from eq 3. Error is ±0.1 Å.

build-up rates to d2-PPA and d2-CEPA, and comparable values of T_{IS} are extracted from fits to the I−S model of the initial build-up behavior (see Table 2). This strongly indicates that the proton proximity between phosphorus and the acidic protons in the deuterated samples and capped samples is similar, confirming complete absence of the acidic protons

in agreement with the ¹H MAS NMR results (Figure 6). The different sites in the nanoparticle samples displayed indistinguishable build-up behavior when integrated intensities of the different components were used. A stack plot of the ³¹P CP-MAS NMR spectra of CEPA capped SnO₂ nanoparticles as a function of contact time is presented to compare with the plotted build-up behavior (see Supporting Information, Figure S4). It is assumed that the mobility is comparable between the pure deuterated phosphonic acids and the ones linked to the nanoparticle surface. This appears to be a safe assumption because the intensity of the spinning sideband manifolds observed in the ¹H MAS experiments are alike, thus, the ¹H-¹H dipolar coupling can be considered comparable. A dynamic averaging of this coupling would be expected if the mobility differed between the pure phosphonic acid and the capped nanoparticle samples.

The ³¹P CP-MAS build-up curves display dipolar oscillations indicative of coherent polarization transfer from the nearest proton to the phosphorus nuclei. Such behavior is typically observed in single-crystal samples,[26,28] peptide samples in oriented lipid bilayers,[55] or well isolated spin pairs.[33] Recently, there have been a few examples where dipolar oscillations have been observed in ³¹P CP-MAS build-up curves where higher MAS speeds (≥10 kHz) are utilized to suppress the effect of proton spin-diffusion that usually smears the observation of dipolar oscillations.[34−36] In these studies, it was possible to obtain the distance between the proton and phosphorus in a P−H and P−O−H group from the dipolar coupling. The following equation can be implemented to calculate the distance between a spin pair from the dipolar coupling:

$$b_{IS} = \frac{\mu_0 \hbar \gamma_I \gamma_S}{4\pi r_{IS}{}^3} \qquad (3)$$

where r_{IS} is the internuclear distance between the two spins, γ_I and γ_S are the gyromagnetic ratios of the heteronuclear coupled spins, μ_0 is the vacuum permeability, and $\hbar$ is the Planck constant.[56]

The dipolar oscillation observed for the pure CEPA and PPA samples is a direct result of coherent polarization transfer in the P−O−H group allowing for an accurate measurement of the dipolar coupling constant by fitting the build-up curve to the I−I*−S model. The P−O−H distance

(55) Tian, F.; Cross, T. A. *J. Magn. Reson.* **1997**, *125*, 220−223.
(56) Schmidt-Rohr, K.; Spiess, H. W. *Multidimensional Solid-State NMR and Polymers*; Academic Press: London, 1994.
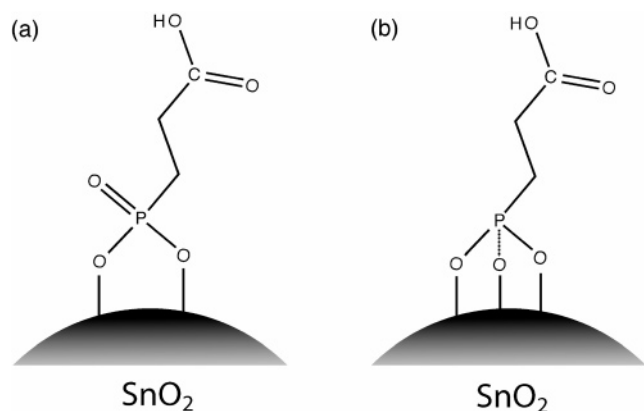
Figure 8. Phosphonic acid bonding modes at the SnO₂ nanoparticle interface, (a) bidentate and (b) tridentate.

is then calculated from D with eq 3. The X-ray structure[57] of PPA is known, and this sample can be used to compare the distance extracted from the dipolar coupling with eq 3. Excellent agreement is observed between the 2.15 Å distance determined from the dipolar coupling constant and the average distance of 2.2 Å reported by XRD. For CEPA, the X-ray structure is not known, but a similar distance is determined compared to PPA, which is consistent with a P−O−H group. In the deuterated and capped nanoparticle samples, weaker oscillations are observed that could also be fit with the I−I*−S model. In the case of PPA, the distance matches perfectly to the nearest proton on the phenyl ring, which is at a distance of 2.96 Å from the XRD structure.[57] This is consistent with the complete deprotonation of the phosphonic acid group upon capping and shows that it is possible to obtain distances at even longer range compared to the P−H and P−O−H distances previously determined with this technique.[34−36] For d2-CEPA and CEPA capped SnO₂ nanoparticles, a closer distance is extracted compared to the d2-PPA and PPA capped nanoparticles. Although the X-ray structure of CEPA is not known, the structure of a closely related molecule ethane-1,2-diphosphonic acid has been determined.[58] The distance measured from CP on d2-CEPA and CEPA capped SnO₂ nanoparticles is consistent with the closest CH₂ group that is at a distance of 2.3 Å in ethane-1,2-diphosphonic acid.

The results of the ³¹P CP build-up curves and ¹H MAS NMR strongly indicate that neither of the two primary phosphonic acid sites observed in the ³¹P CP-MAS NMR spectra of CEPA and PPA capped SnO₂ nanoparticles are protonated. These two ³¹P resonances are shifted 6−7 and 12−13 ppm upfield from the chemical shift of the pure phosphonic acid. Similar ³¹P resonance shifts have been observed in numerous studies where phosphonic acids were reacted with silica,[47,48] guanidine functionalized silica,[49] and ZrO₂.[23,24,43] This indicates that it is probably not differences in the surface that cause the shift but more likely the binding modes of the phosphonic acid. IR spectra (data not shown) display a noteable decrease in the intensity of the P=O stretching band in both CEPA and PPA capped nanoparticles. Therefore, it appears likely that the resonance shifted 6−7 ppm and 12−13 ppm upfield are best assigned to bi- and tridentate bonding modes, respectively (see Figure 8).

Conclusions

In conclusion, phosphonic acids appear to be excellent ligands for the capping of metal oxide nanoparticles. The phosphonic acid can be chosen to have a terminal functional group such as a carboxylic acid to render the normally insoluble nanoparticles soluble in aqueous solutions. This not only permits characterization via solution state NMR but also allows the nanoparticles to be utilized in applications where aqueous solubility is a requirement. ¹H MAS NMR and ³¹P CP build-up behavior greatly assisted in assigning two primary ³¹P resonances to bi- and tridentate bonding modes of phosphonic acids at the SnO₂ nanoparticle interface. Dipolar oscillations in the CP build-up curves could be used to extract accurate distances and confirm the degree of protonation of the phosphonic acid groups. NMR proved to be a useful tool to characterize the ligand structure of phosphonic acid capped metal oxide nanoparticles in both solution and the solid state.

Supporting Information Available: EDX spectrum of CEPA capped SnO₂ nanoparticles, ¹H solution NMR spectra of CEPA capped SnO₂ nanoparticles with and without hole burning, TGA of CEPA and PPA capped SnO₂ nanoparticles, and horizontally stacked ³¹P CP-MAS NMR spectra of CEPA capped SnO₂ nanoparticles collected on the −1 spinning sideband in the Hartmann−Hahn matching profile as a function of CP contact time (PDF). This material is available free of charge via the Internet at http://pubs.acs.org.

CM062821U

(57) Weakley, T. J. R. *Acta Crystallogr., Sect. B* **1976**, *32*, 2889−2890.
(58) Peterson, S. W.; Gebert, E.; Reis, A. H., Jr.; Druyan, M. E.; Mason, G. W.; Peppard, D. F. *J. Phys. Chem.* **1976**, *81*, 466−471.